CRYSTAL GROWTH & DESIGN

Article

Chiral Cd(II) coordination polymers based on amino acid derivatives: the effect of side chain on structure

Hui Min Tay, and Carol Hua

Cryst. Growth Des., **Just Accepted Manuscript** • DOI: 10.1021/acs.cgd.0c00468 • Publication Date (Web): 21 Jul 2020

Chiral Cd(II) coordination polymers based on amino acid derivatives: the effect of side chain on structure

*Hui Min Tay and Carol Hua**

School of Chemistry, The University of Melbourne, Parkville, Victoria, 3010, Australia. *E-mail: carol.hua@unimelb.edu.au

Abstract

Homochiral coordination polymers have emerged as promising candidates for a range of chirotechnological applications, including asymmetric catalysis and enantioselective separation. The use of ligands derived from naturally occurring L-amino acids is an inexpensive and effective approach to generate a range of homochiral coordination polymers. To investigate the structure-directing effect of the amino acid side chain, seven homochiral Cd(II) frameworks were synthesised using semi-rigid dicarboxylates composed of L-amino acids appended to terephthalic acid (H_2TMXxx, where Xxx = Ala, Val, Phe, Trp, Tyr and His) and bis(4-pyridyl)ethylene co-ligands. When Xxx = Val, Tyr, Phe or Trp, a series of 2D (4,4)-networks were obtained, in which the different intermolecular interactions of the side chains result in subtle changes in crystal packing. Employing Xxx = Ala or Tyr led to 3D frameworks with a $\{6^5 \cdot 8\}$ topology, in which the varying steric bulk of the side chains results in significant differences in framework geometry as well as the shape and volume of the solvent-accessible channels. When Xxx = His, the imidazole side chains coordinate to the metal centre to direct the formation of a 3D pillared structure that undergoes two-fold interpenetration.

Introduction

Chirality is prevalent throughout nature, with most biologically important molecules, including amino acids, nucleotides and sugars, occurring predominantly as a single enantiomer. The enantiomers of a chiral molecule may interact differently with enzymes, receptors and other chiral biomolecules, giving rise to different biological effects.[1, 2] This behavior is exemplified in the two enantiomers of dopamine; *L*-dopamine is used to treat Parkinson's disease while *D*-dopamine elicits neurotoxic side effects.[3] Obtaining enantiomerically pure chiral molecules is therefore of

great importance in the pharmaceutical industry, with nearly 50% of drugs on the market being chiral molecules.[4, 5] Motivated by the high demand for enantiopure drugs, significant research effort has been devoted to developing methods for the preparation of chiral molecules.[4, 6, 7]

Homochiral coordination polymers have emerged as a promising class of materials with various applications in chirotechnology, including as asymmetric catalysts[8-12] or chiral stationary phases for the chromatographic separation of racemic mixtures.[13-16] Frameworks containing large solvent-accessible chiral pores are particularly promising as the environment in the pores can be altered by changing the inorganic ions and chiral organic ligands, thereby tailoring the framework towards specific chiral substrates.[17] However, the large-scale preparation of homochiral frameworks in an inexpensive and reproducible manner remains a considerable challenge.[18] The use of enantiopure organic linkers is currently the most direct and reliable method of introducing chirality into frameworks, but this approach is synthetically demanding as the organic linkers used often require multi-step syntheses with prohibitively low overall yields.[19-22] Another approach involves combining metal ions and achiral ligands in the presence of a chiral template in order to direct the formation of a homochiral network.[23-25] A major limitation of this approach, however, is the difficulty of systematically predicting and controlling the enantiomeric excess of the reaction products.

A reliable and inexpensive strategy for preparing homochiral coordination polymers is to use ligands derived from commercially available chiral molecules.[26-28] The family of naturally-occurring α-amino acids are promising candidates for chiral precursors as they are non-toxic, inexpensive and can be readily obtained in high enantiopurity.[29] The structural flexibility of α-amino acids, which may hinder the formation of robust porous frameworks, can be reduced by functionalisation with suitable rigid aromatic units.[30-32] A straightforward implementation of this strategy involves appending a benzoate group to the *N*-terminus of the amino acid, which can be achieved in two synthetic steps to obtain semi-rigid terephthaloyl mono amino acid linkers (H_2TMXxx, Xxx = amino acid). Five homochiral frameworks, some of which contain significant pore space (up to 2968 Å^3 per unit cell or 36.2% of the crystal volume), have been constructed using the alanine-derived ligand (H_2TMAla),[30] demonstrating the propensity of H_2TMXxx linkers to promote the formation of porous homochiral coordination polymers. The inclusion of rigid N-donor co-ligands was used to further increase the dimensionality and porosity of the frameworks.

The side chain of alanine consists of a single methyl group, making it the simplest of the 19 chiral naturally-occurring α-amino acids. The other α-amino acids contain a variety of side chains capable of participating in different intermolecular interactions, including hydrophobic interactions, π-stacking, electrostatic interactions and metal coordination. The diversity of functional groups available within the family of α-amino acids therefore offers opportunities for tuning the structure and properties of the homochiral coordination polymers simply by changing the amino acid precursor.

To investigate the effect of varying the amino acid side chain on the structure of the resulting coordination polymers, H_2TMAla and five novel H_2TMXxx ligands were synthesised using the amino acid precursors: valine (Val), phenylalanine (Phe), tyrosine (Tyr), tryptophan (Trp) and histidine (His). Combining the H_2TMXxx ligands with Cd(II) and the rigid dipyridyl bis(4-pyridyl)ethylene (bpee) co-ligand yielded seven 2D and 3D homochiral coordination polymers. Single-crystal X-ray diffraction studies on the coordination polymers revealed the important structure-directing role of the amino acid side chains, which ranged from exerting a subtle influence on the crystal packing to dramatically altering the dimensionality of the framework.

Experimental section

General Considerations

All chemicals and solvents were used as obtained and without further purification. Distilled dichloromethane (dried over CaH_2) was used in all experiments requiring anhydrous dichloromethane.

NMR spectra (^{1}H and ^{13}C{^{1}H}) were recorded on a Varian MR400 spectrometer operating at 400 MHz for ^{1}H and 100 MHz for ^{13}C. ^{1}H and ^{13}C chemical shifts were referenced internally to residual solvent resonances. High resolution electrospray ionisation (ESI) mass spectra were acquired as solution samples in a methanol/formic acid mixture or in acetonitrile (~1 ppm) on an Agilent 6520 Accurate-Mass Q-TOF spectrometer. Fourier Transform Infrared spectra were measured on a Bruker Alpha spectrometer between 4000 – 400 cm^{-1} with 4 cm^{-1} resolution and 32 scans and normalised as absorbance spectra. Thermal gravimetric analysis was conducted on a Mettler Toledo TGA/SDTA851 instrument using aluminum crucibles as sample holders under high purity nitrogen. Typical analysis involved heating the sample up to 450 °C with a temperature increment

of 4 °C min^{-1}. Microanalysis was carried out at the Chemical Analysis Facility – Elemental Analysis Service in the Department of Chemistry and Biomolecular Science at Macquarie University, Australia.

Single crystal X-ray diffraction data was collected on a Rigaku Oxford Diffraction Synergy-S diffractometer equipped with CuKα radiation or on the MX1 or MX2 beamline at the Australian Synchrotron.[33, 34] In general, single crystals were transferred directly from the mother liquor into immersion oil and placed under a stream of nitrogen at 100 K or 240 K. Crystal structures were solved by direct methods using the program SHELXT[35] and refined using a full matrix least-squares procedure based on F^2 (SHEXL),[36] within the Olex2[37] GUI program. In structures containing disordered solvent molecules that could not be satisfactorily modelled, the solvent mask routine in Olex2 was used.[38]

Framework Synthesis

$[Cd_2(TMVal)_2(bpee)_2]\cdot 0.8DMF\cdot 3.9H_2O$ (1). A solution of H_2TMVal (8.0 mg, 0.03 mmol), bis(4-pyridyl)ethylene (5.5 mg, 0.03 mmol) and $Cd(NO_3)_2\cdot 4H_2O$ (27.8 mg, 0.09 mmol) in DMF/H_2O (3 mL, 1:1 v/v) was heated at 80 °C for 2 days. The reaction mixture was cooled to room temperature, filtered and washed with 1:1 DMF/H_2O (5 mL) to obtain colourless needles (12.9 mg, 64%). IR (ATR): 3055, 2960, 2873, 1669, 1635, 1604, 1545, 1399, 1302, 1094, 1014, 985, 874, 832, 777, 661, 551, 472 cm^{-1}. Elemental analysis (%): calcd for $C_{52.8}H_{59.4}Cd_2N_{6.8}O_{14.7}$: C 50.76, H 4.79, N 7.62; found: C 50.58, H 4.77, N 7.66.

$[Cd_2(TMTyr)_2(bpee)_2]\cdot 1.6DMF\cdot 2.3H_2O$ (2). A solution of H_2TMTyr (9.9 mg, 0.03 mmol), bpee (5.5 mg, 0.03 mmol) and $Cd(NO_3)_2\cdot 4H_2O$ (9.3 mg, 0.03 mmol) in DMF/H_2O (3 mL, 1:2 v/v) was heated at 80 °C for 7 days. The reaction mixture was cooled to room temperature, filtered and washed with 1:1 DMF/H_2O (5 mL) to obtain colourless needles (9.1 mg, 44%). IR (ATR): 3060, 2918, 1670, 1642, 1605, 1583, 1516, 1392, 1267, 1066, 1016, 979, 833, 736, 658, 550, 497 cm^{-1}. Elemental analysis (%): calcd for $C_{62.8}H_{58.8}Cd_2N_{7.6}O_{15.9}$: C 53.91, H 4.24, N 7.61; found: C 53.92, H 4.27, N 7.64.

$[Cd_4(TMPhe)_4(bpee)_4]\cdot 2.3DMF\cdot 6.4H_2O$ (3). A solution of H_2TMPhe (9.4 mg, 0.03 mmol), bpee (5.5 mg, 0.03 mmol) and $Cd(NO_3)_2\cdot 4H_2O$ (9.3 mg, 0.03 mmol) in DMF/H_2O (3 mL, 1:1 v/v) was heated at 80 °C for 5 days. The reaction mixture was cooled to room temperature, filtered and

washed with 1:1 DMF/H_2O (5 mL) to obtain colourless needles (13.4 mg, 68%). IR (ATR): 3057, 2919, 1665, 1605, 1585, 1542, 1387, 1096, 1017, 832, 737, 700, 549, 499 cm^{-1}. Elemental analysis (%): calcd for $C_{122.9}H_{118.9}Cd_4N_{14.3}O_{28.7}$: C 54.56, H 4.43, N 7.41; found: C 54.57, H 4.35, N 7.41.

$[Cd_3(TMTrp)_2(bpee)_3(formate)_2]\cdot 2.6DMF\cdot 7H_2O$ (4). A solution of H_2TMTrp (10.6 mg, 0.03 mmol), bis(4-pyridyl)ethylene (5.5 mg, 0.03 mmol), sodium formate (1.0 mg, 0.015 mmol) and $Cd(NO_3)_2\cdot 4H_2O$ (9.3 mg, 0.03 mmol) in DMF/H_2O (3 mL, 5:1 v/v) was heated at 80 °C for 5 days. The reaction mixture was cooled to room temperature, filtered and washed with DMF (5 mL) to obtain fine colourless needles (16.7 mg, 64%). IR (ATR): 3372, 3053, 2929, 1656, 1605, 1584, 1517, 1487, 1402, 1252, 1067, 1014, 972, 827, 741, 549 cm^{-1}. Elemental analysis (%): calcd for $C_{83.9}H_{88.3}Cd_3N_{12.6}O_{23.6}$: C 50.69, H 4.48, N 8.88; found: C 50.65, H 4.61, N 8.89.

$[Cd_4(TMAla)_4(bpee)_4]\cdot 2DMF\cdot 12.2H_2O$ (5). A solution of H_2TMAla (7.1 mg, 0.03 mmol), bis(4-pyridyl)ethylene (5.5 mg, 0.03 mmol) and $Cd(NO_3)_2\cdot 4H_2O$ (9.3 mg, 0.03 mmol) in DMF/H_2O (3 mL, 1:1 v/v) was heated at 80 °C for 5 days. The reaction mixture was cooled to room temperature, filtered and washed with 1:1 DMF/H_2O (5 mL) to obtain colourless octahedral blocks (7.1 mg, 38%). IR (ATR): 3360, 2923, 1649, 1603, 1585, 1534, 1390, 1284, 1067, 1012, 830, 806, 551 cm^{-1}. Elemental analysis (%): calcd for $C_{98}H_{114.4}Cd_4N_{14}O_{34.2}$: C 47.36, H 4.64, N 7.89; found: C 47.36, H 4.46, N 7.47.

$[Cd_2(TMTyr)_2(bpee)_2]\cdot 2DMF\cdot 7.7MeOH$ (6). A solution of H_2TMTyr (9.9 mg, 0.03 mmol), bis(4-pyridyl)ethylene (5.5 mg, 0.03 mmol) and $Cd(NO_3)_2\cdot 4H_2O$ (9.3 mg, 0.03 mmol) in DMF/MeOH (3 mL, 2:1 v/v) was heated at 80 °C for 24 hours. The reaction mixture was cooled to room temperature and washed with 1:1 DMF/H_2O (3 × 4 mL) to remove the white amorphous powder. The remaining solid was filtered and washed with 1:1 DMF/H_2O (5 mL) to obtain colourless cube-like crystals (10.2 mg, 37%). IR (ATR): 3291, 2926, 2916, 1658, 1605, 1582, 1535, 1512, 1386, 1294, 1246, 1092, 973, 877, 805, 739, 665, 512 cm^{-1}. Elemental analysis (%): calcd for $C_{72.7}H_{89.8}Cd_2N_8O_{21.7}$: C 52.99; H 5.49; N 6.80; found: C 53.01, H 4.31, N 6.80.

$[Cd(TMHis)(bpee)]\cdot DMF\cdot 3H_2O$ (7). A solution of H_2TMHis (9.1 mg, 0.03 mmol), bis(4-pyridyl)ethylene (5.5 mg, 0.03 mmol) and $Cd(NO_3)_2\cdot 4H_2O$ (9.3 mg, 0.03 mmol) in DMF/H_2O (3 mL, 1:1 v/v) was heated at 80 °C for 2 days. The reaction mixture was cooled to room temperature and washed with 1:1 DMF/H_2O (3 × 4 mL) to remove the white amorphous powder. The remaining solid was filtered and washed with 1:1 DMF/H_2O (5 mL) to obtain colourless block crystals (11.1

mg, 51%). IR (ATR): 3536, 3413, 3132, 3058, 2997, 2868, 1664, 1638, 1605, 1579, 1494, 1385, 1332, 1283, 1104, 1013, 989, 955, 841, 839, 745, 657, 550, 467, 445 cm^{-1}. Elemental analysis (%): calcd for $C_{29}H_{34}CdN_6O_9$: C 48.18; H 4.74; N 11.62; found: C 48.05, H 4.74, N 11.43.

Results and Discussion

Synthesis of H_2TMXxx

A two-step synthetic route was employed to synthesise the H_2TMXxx ligands. This involves an amide coupling between monomethyl terephthaloyl acid chloride and the appropriate L-amino acid methyl ester, followed by hydrolysis of the two methyl ester groups (**Scheme 1**). When Xxx = Ala, Val, Phe or Trp, the desired product was obtained in 73-81% overall yield (**Table 1**). However, when Xxx = His or Tyr, the nucleophilic side chains also reacted with monomethyl terephthaloyl acid chloride to give disubstituted intermediates. The terephthaloyl group appended to the side chain was hydrolysed in the subsequent step to yield the desired product. This generated terephthalic acid as a by-product, which was removed by column chromatography (Xxx = Tyr, 81%) or by exploiting the greater water solubility of the ligand under acidic conditions (Xxx = His, 25%).

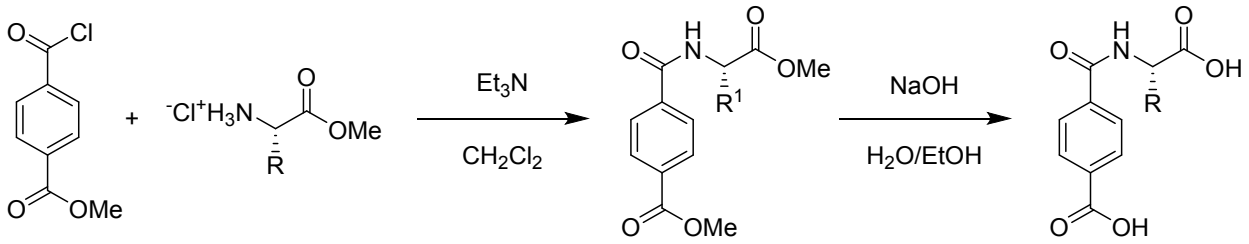

Scheme 1. Synthetic scheme for the preparation of H_2TMXxx ligands

Table 1. Synthetic yield (%) of compounds **1a-f** and **2a-f** with structures of side chains

	R^1	Yield of 1 (%)	R	Yield of 2 (%)
a	-CH_3	82	-CH_3	95
b	-*i*Pr	84	-*i*Pr	90
c	-Bn	90	-Bn	90
d	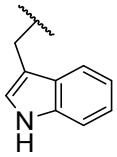	99	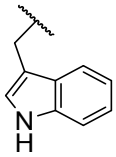	74
e	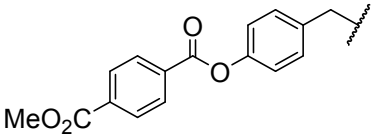	77	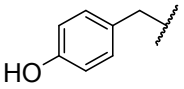	33
f	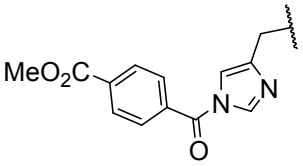	87	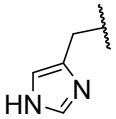	93

Framework Synthesis

Seven homochiral coordination polymers (**1-7**) were synthesised via the solvothermal reaction of H_2TMXxx with $Cd(NO_3)_2 \cdot 4H_2O$ and bpee in solvent mixtures of DMF/water or DMF/methanol at 80 °C. A stoichiometric ratio of 1:1:1 $Cd(NO_3)_2$: H_2TMXxx: bpee was consistently used for the initial syntheses. However, for some compounds, increasing the concentration of $Cd(NO_3)_2 \cdot 4H_2O$ enabled higher yields to be obtained. Powder XRD experiments were used to verify that the structure of the coordination polymer was unchanged.

2D Networks with Xxx = Val, Phe, Tyr and Trp (1-4).

The reactions of H_2TMXxx, where Xxx = Val, Phe and Tyr, with bpee in a mixture of DMF and water yielded colourless needle crystals which were found to be 2D rectangular sheet structures of

composition [Cd(TMXxx)(bpee)]·xDMF·yH_2O (Xxx = Val (**1**), Tyr (**2**), Phe (**3**)). The structures of **1**-**2** were solved in the monoclinic space group $P2_1$ while **3** was solved in the triclinic space group $P\bar{1}$. The inorganic node in **1-3** is a $Cd_2(COO)_4N_4$ cluster connecting four $TMXxx^{2-}$ ligands and four bpee ligands (**Figure 1**).

In **1**, the two crystallographically distinct Cd(II) atoms are both six-coordinate with a distorted octahedral coordination environment, as determined using the SHAPE[39] program. The four equatorial sites of each Cd(II) are occupied by oxygen atoms from the carboxylate groups of three $TMXxx^{2-}$ ligands, one of which binds in a chelating mode while the other two serve as a three-atom bridge that connects the two Cd(II) centres. The axial positions of the Cd(II) ion are occupied by pyridyl nitrogen atoms from two bpee ligands (**Figure 1a**). The Cd(II)-O bond lengths vary from 2.250(6) Å to 2.412(6) Å and the Cd(II)-N bond lengths fall in the range of 2.280(8) Å to 2.33(1) Å. These bond lengths are consistent with reported structures containing six-coordinate Cd(II) centres.[40]

In contrast, the $Cd_2(COO)_4N_4$ clusters in **2** contain a six-coordinate Cd1 and a seven-coordinate Cd2, which were calculated using SHAPE[39] to possess a distorted octahedral and pentagonal bipyramidal coordination geometry respectively. The Cd(II)-O bond lengths for Cd1 range from 2.249(4) Å to 2.470(6) Å, typical of six-coordinate Cd(II), while the corresponding distances for Cd2 are increased, ranging from 2.329(7) Å to 2.528(6) Å, consistent with the presence of a seven-coordinate Cd(II) centre.[40] The oxygen atoms O43 and O19, which are coordinated to Cd1 and belong to the bridging carboxylate groups, form an O-Cd-O angle of 124.5°. The corresponding oxygen atoms bound to Cd2 (O42 and O18) form a significantly larger O-Cd-O angle of 137.4°. The large difference in the two O-Cd-O angles positions O43 at a distance of 2.311(5) Å from Cd1 and 2.454(6) Å from Cd2, sufficiently close to coordinate to both Cd(II) centres and act as a μ_2 bridge. This increases the coordination number of Cd2 from six to seven (**Figure 1b**). In contrast, the corresponding O-Cd-O angles in **1** are similar (128.4° for Cd1 and 125.8° for Cd2), giving rise to two six-coordinate Cd(II) centres with no μ_2-O bridge.

Compound **3** contains two types of $Cd_2(COO)_4N_4$ clusters, one of which contains two six-coordinate Cd(II) centres, similar to **1**, while the other contains a six-coordinate and a seven-coordinate Cd(II) centre, similar to **2**. As before, the coordination geometries for the six- and seven-coordinate Cd(II) centres were calculated to be distorted octahedral and pentagonal

bipyramidal respectively. [39] The Cd(II)-O bond lengths fall in the range 2.233(8)-2.558(7) Å for the six-coordinate Cd(II) centres (Cd1, Cd2 and Cd3) and 2.318(9)-2.611(8) Å for the seven-coordinate Cd(II) centre (Cd4). Equivalent clusters are connected by $TMPhe^{2-}$ ligand pairs while inequivalent clusters are linked via bpee ligands.

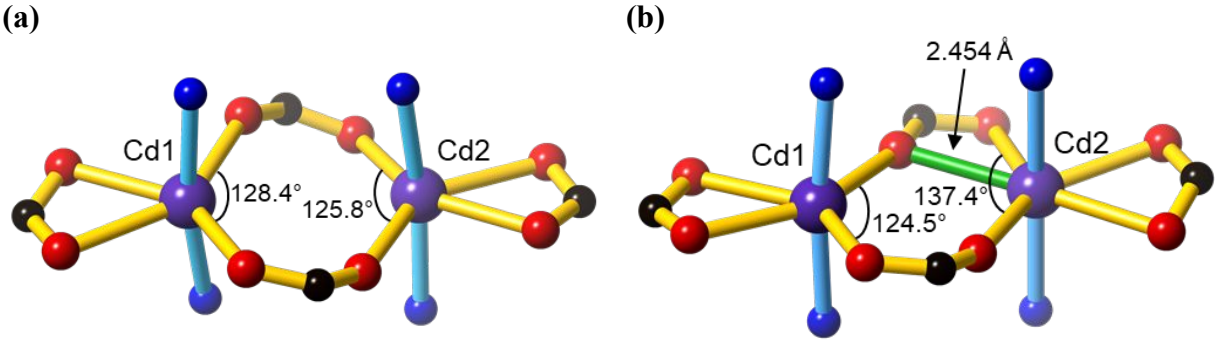

Figure 1. The $Cd_2(COO)_4N_4$ cluster in (a) **1**, in which both Cd1 and Cd2 are six-coordinate; (b) **2**, in which Cd1 is six-coordinate while Cd2 is seven-coordinate. The Cd2-O43 bond is highlighted in green. Atoms are depicted as follows in parts a-b: cadmium (purple), oxygen (red), nitrogen (blue) and carbon (black).

In **1**-**3**, adjacent clusters are linked by pairs of $TMXxx^{2-}$ ligands to form a double chain in which the $TMXxx^{2-}$ ligands on each side of the chain are arranged in a head-to-tail manner and run anti-parallel to the ligands on the opposite side of the chain (**Figure 2a**). These anti-parallel double chains are bridged by pairs of bpee ligands to form sheets with an sql topology and Schläfli symbol $\{4^4 \cdot 6^2\}$ [41] (**Figure 2b**). The sheets are stacked in a staggered manner to give narrow channels, which are occupied by solvent molecules (**Figure 2c**). In **2** and **3**, some of these solvent molecules were disordered and could not be satisfactorily modelled, hence the solvent mask routine within Olex2 was employed.[38] The asymmetric unit of **2** was estimated to contain 91 residual electrons, which is in good agreement with the proposed solvent content of 1.6 DMF and 2.3 H_2O. The structure of **3** contains 2 DMF and 4 H_2O molecules that were well-ordered, as well as 41 residual electrons from disordered solvent. This corresponds well to the proposed solvent content of 2.3 DMF and 6.4 H_2O molecules.

Evacuation of the channels would give a total void space of 22% in **1** and 14% in **2** and **3**. The lower potential void space in **2** and **3** can be attributed to the bulkier aromatic side chains in phenylalanine and tyrosine compared to the isopropyl side chain of valine. The thermal gravimetric analysis (TGA) of **1** (**Figure S8**) indicates a mass loss of 4.5% between 30 and 105 °C, which corresponds to the loss of 3.3 H_2O molecules per asymmetric unit, followed by a further

mass loss of 4.5% between 110-195 °C, corresponding to 0.8 DMF molecules. There is a plateau in the TGA trace from 195 – 290 °C, indicating framework stability, before the framework decomposes about 290 °C. The TGA trace of **2** contains a gradual mass decrease of 3.6% between 70 and 226 °C, which may correspond to 2.3 H_2O and 0.1 DMF molecules. In **3**, there is a gradual mass loss of 8.3% from 60-260 °C, which may correspond to the loss of 6.4 H_2O molecules and 1.5 DMF molecules per asymmetric unit. Framework decomposition occurs at 295 °C in **2** and 330 °C in **3**.

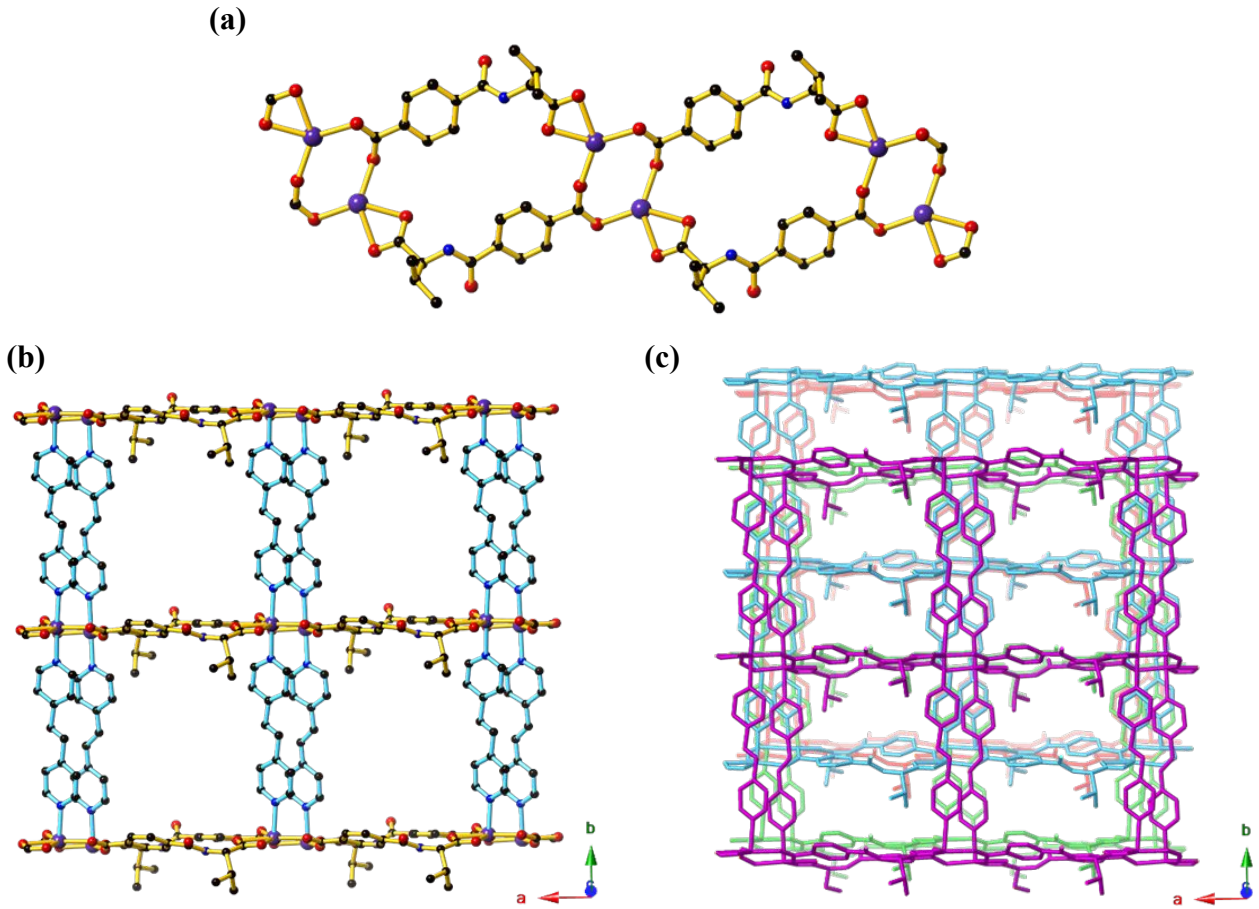

Figure 2. Structure of [Cd(TMVal)(bpee)]·xDMF·yH_2O (**1**) showing (a) the double chain formed by linking adjacent Cd(II) clusters with anti-parallel pairs of $TMVal^{2-}$ ligands; (b) a single sheet viewed along the *c* axis; (c) a view of the framework down the *c* axis, showing the staggered packing of the sheets. Atoms are depicted as follows in parts a-b: cadmium (purple), oxygen (red), nitrogen (blue) and carbon (black). Hydrogens have been omitted for clarity.

Despite the similar bonding and connectivity within each (4,4)-sheet in **1**-**3**, there are subtle differences in the packing of the sheets, resulting from conformational differences in the amino acid side chains. In **3**, there are four crystallographically distinct $TMPhe^{2-}$ ligands which differ markedly in the position and orientation of the benzyl side chain, as seen from a comparison of the

torsion angles in the four types of $TMPhe^{2-}$ ligands (**Table 2**). In particular, there are large variations in the torsion angles defined by C_0-N-C_α-C_β, which range from +75.41° to +144.67°, and N-C_α-C_β-C_γ, which range from −58.98° to +56.53°. In contrast, **1** and **2** crystallise in the higher symmetry space group $P2_1$ and contain two crystallographically inequivalent $TMXxx^{2-}$ ligands. Within each structure, the two types of $TMXxx^{2-}$ ligands have similar C_0-N-C_α-C_β and N-C_α-C_β-C_γ torsion angles, differing by a maximum of 22.38° and 2.81° respectively (**Table 2**).

Table 2. Torsion angles of $TMXxx^{2-}$ ligands in the crystal structures of **1**-**3**

Structure	Ligand Colour[1]	C_{arom}-C_0-N-C_α (°)	C_0-N-C_α-C_β (°)	N-C_α-C_β-C_γ (°)
1	Red	+175.98	+92.57	−59.22, +66.33
1	Blue	-179.60	+101.35	−58.35, +65.66
2	Red	−176.47	+114.20	−67.47
2	Blue	−173.96	+136.58	−64.66
3	Red	−165.78	+102.16	−58.98
3	Blue	−165.96	+144.67	−56.95
3	Green	+176.77	+75.41	+48.03
3	Purple	−173.03	+91.99	+56.53

[1]Corresponds to the colour displayed in **Figure 3a**.

The large differences in the orientation of the benzyl side chains in **3** can be attributed to the large number of possible non-covalent interactions that can be formed between the benzyl groups of $TMPhe^{2-}$ and neighbouring components of the framework (**Figure 3a**). This includes various π-π stacking and CH-π interactions at distances of 3.5-4.0 Å. In contrast, there are fewer variations in the intermolecular interactions involving the $TMVal^{2-}$ and $TMTyr^{2-}$ side chains in **1** and **2**. The isopropyl side chains of the $TMVal^{2-}$ ligands in **1** form CH-π interactions with the pyridyl rings of adjacent bpee ligands with distances of 3.609 Å and 3.851 Å. Although the phenol side chains of the $TMTyr^{2-}$ ligands in **2** also have the propensity to form π-π stacking and CH-π interactions, the predominant interaction appears to be hydrogen bonding between the phenol hydroxyl group and the amide oxygen of a neighbouring sheet, with H-bond distances of 2.64(1) Å and 2.85(2) Å. These directional interactions restrict the conformations adopted by the side chains in the $TMXxx^{2-}$ ligands of **1** and **2** (**Figure 3b**).

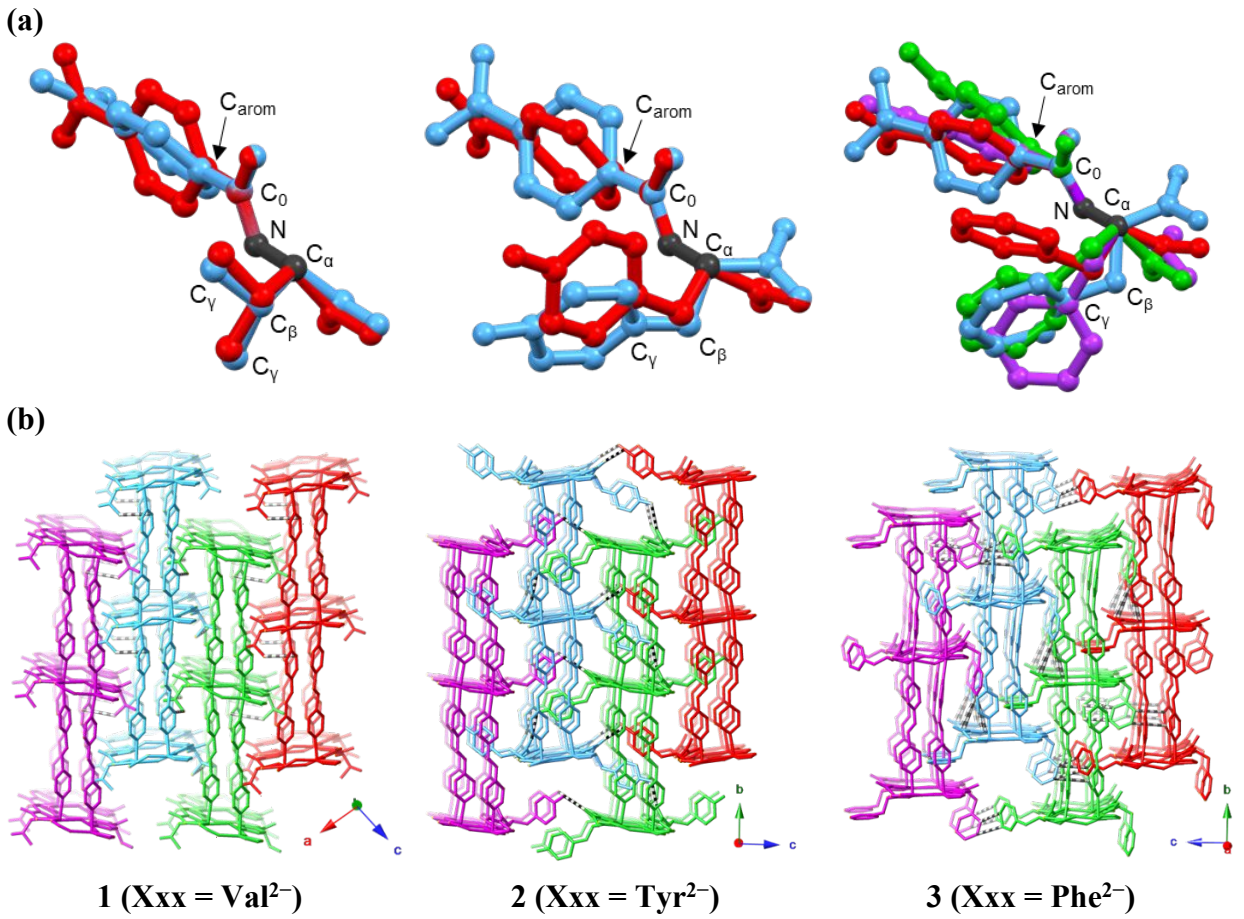

Figure 3. (a) An overlay of the crystallographically inequivalent ligands in **1**-**3**, showing the different arrangement of groups about the N-C_α bond (highlighted in black); (b) The crystal packing in **1**, **2** and **3**, with individual sheets represented in purple, blue, green and red. Intermolecular interactions involving the side chains, including hydrogen bonding interactions (in **2**) and short contacts in the range of 3.5-4.0 Å (in **1** and **3**) are represented by grey and black bands.

The reaction of H_2TMTrp with $Cd(NO_3)_2{\cdot}4H_2O$ and bpee under similar reaction conditions resulted in an inhomogeneous mixture formed after seven days, which contained pale orange needles suitable for analysis by X-ray diffraction. This unexpectedly revealed a 2D coordination polymer of composition $[Cd_3(TMTrp)_2(bpee)_3(formate)_2]$ (**4**), which crystallised in the space group $P2_1$. The formate ions have likely formed from the hydrolysis of DMF at high temperatures.[42] Upon the addition of sodium formate to the reaction mixture, homogenous microcrystalline needles separated after two days, which were confirmed by PXRD to be the same compound. Remarkably, although **4** differs significantly in composition from **1-3** due to the inclusion of formate ions, SCXRD studies of **4** revealed a 2D (4,4)-sheet[41] structure topologically identical to that of **1-3** (**Figure 4**).

The structure of **4** differs from **1-3** predominantly in the inorganic node, with **4** containing a linear $Cd_3(COO)_6N_6$ cluster (**0a**). The central Cd(II) atom (Cd1) is located on the site of a pseudo-inversion centre and was found to possess an octahedral coordination environment.[39] Two of its four equatorial sites, which are situated *trans* to each other, are occupied by oxygen atoms from the carboxylate groups of two $TMTrp^{2-}$ ligands. Each of the $TMTrp^{2-}$ carboxylate groups serve as a three-atom bridge connecting Cd1 to either Cd2 or Cd3. The other two equatorial sites, which also have a *trans* relation to each other, are coordinated by oxygen atoms from two formate ions. Each of these oxygen atoms serves as a μ_2-bridge that links Cd1 to either Cd2 or Cd3. The Cd(II)-O bond distances fall in the range 2.270(6) Å to 2.308(8) Å.

Cd2 and Cd3 are both seven-coordinate with a distorted pentagonal bipyramidal coordination geometry.[39] The five equatorial sites are occupied by carboxylate oxygen atoms from a chelating $TMTrp^{2-}$, a chelating formate ion and a bridging $TMTrp^{2-}$. Most of the Cd(II)-O bond lengths fall in the range 2.298(6)-2.410(7) Å, with the exception of the non-bridging formate oxygen atoms (O32 and O72), which have unusually long Cd(II)-O distances of 2.601(8) Å (Cd2-O32) and 2.574(7) Å (Cd3-O72). Bond distances in this range have been observed in structures containing carboxylate groups chelated to Cd(II)[40] and may indicate a weak Cd(II)-O bonding interaction.

The four $TMTrp^{2-}$ ligands within each cluster bridge adjacent clusters along the *a*-direction to form an antiparallel double chain similar to that in **1-3**. The two axial sites of each cadmium centre are occupied by pyridyl nitrogen atoms from bpee co-ligands, which link double chains in the *b*-direction to form a rectangular grid (**Figure 4b**). Similar to that observed in **1-3**, the sheets in **4** stack in a staggered manner to form channels running parallel to the *c* axis. Despite the large size of the indole side chains in $TMTrp^{2-}$, the side chains do not obstruct the channels; this is due to the formation of extensive CH-π interactions between the indole groups and a triad of bpee ligands on a neighbouring sheet, which forces the indole groups to rotate towards the bpee pillars and away from the rectangular channels, as seen in **Figure 4b**. Due to the conformation of $TMTrp^{2-}$ in **4**, the bulky indole side chains force adjacent sheets further apart, increasing the sheet-to-sheet mean plane separation from approximately 7.5 Å in **1-3** to 9.9 Å in **4** (**Figure 4c**). As a result, **4** has a higher calculated void volume of 34%. The TGA trace of **4** contains stepwise mass losses of 6.1% from 30-85 °C (6.7 H_2O molecules) and 9.9% from 90-210 °C (2.7 DMF molecules), before the framework decomposes above 230 °C.

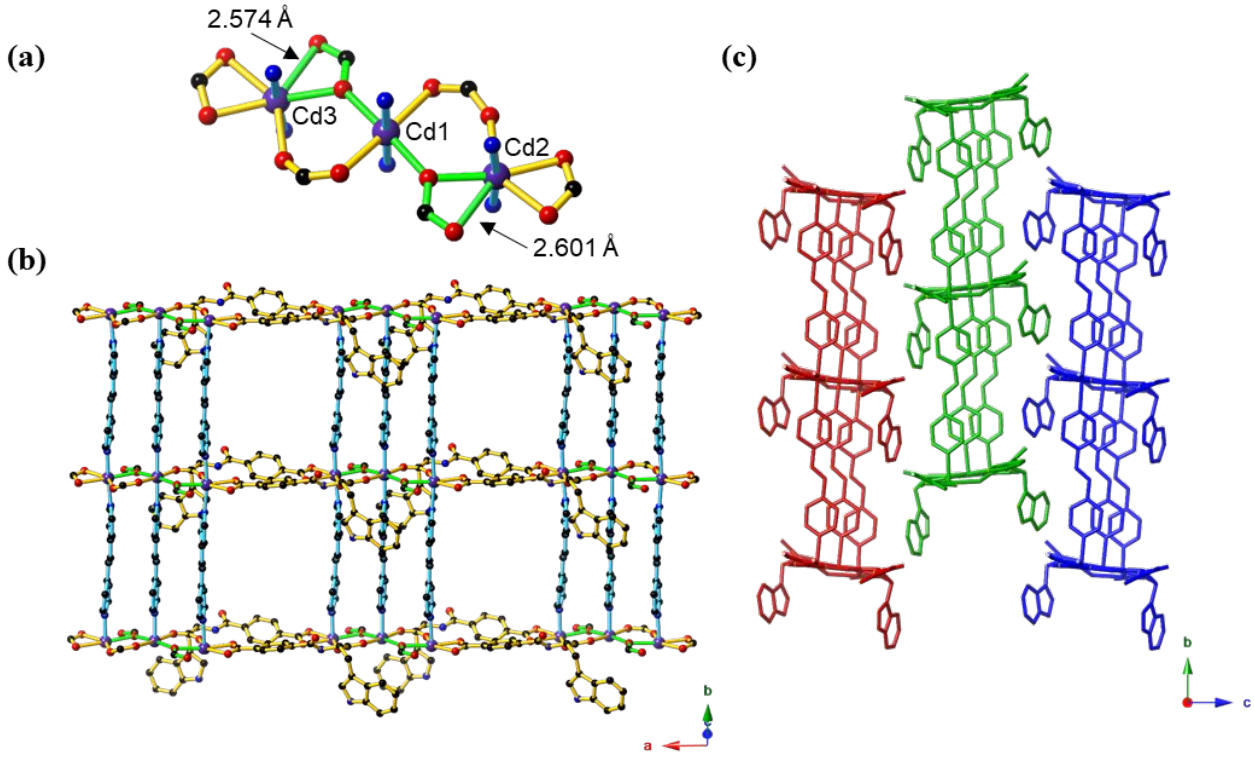

Figure 4. Structure of $[Cd_3(TMTrp)_2(bpee)_3(formate)_2]$ (**4**) showing (a) the trinuclear Cd(II) cluster in **4**, with the bridging formate ligands represented with green bonds, (b) the rectangular grid present in a single sheet and (c) a view along the *a* axis, showing the staggered packing of the sheets with separate sheets represented in red, green and blue. Atoms are depicted as follows in parts a and b: cadmium (purple), oxygen (red), nitrogen (blue) and carbon (black). Hydrogens have been omitted for clarity.

3D Networks with Xxx = Ala and Tyr (5-6).

Combining H_2TMAla or H_2TMTyr with bpee and $Cd(NO_3)_2{\cdot}4H_2O$ in DMF/H_2O or DMF/methanol respectively gives rise to 3D frameworks of composition [Cd(TMXxx)(bpee)] (Xxx = Ala (**5**), Tyr (**6**)) (**Figure 5**). Interestingly, although H_2TMTyr formed a 2D network when combined with Cd(II) and bpee in DMF/H_2O, changing the co-solvent from water to methanol, which has a lower propensity for hydrogen bonding, induced the formation of a different crystalline phase with a rectangular block-like morphology.

The structure of **5** was solved in the monoclinic space group $P2_1$ while **6** was solved in the higher symmetry tetragonal space group $P4_32_12$. Despite the marked differences in space group and unit cell parameters (**5**: a = 14.2809, b = 15.0250, c = 23.6927, β = 101.573°; **6**: $a = b$ = 19.4835, c = 50.6104), both frameworks have the topology of a **sqc5** net with the Schläfli symbol of $\{6^5{\cdot}8\}$.[41]

However, the crystal packing in the two structures differ significantly, which arises from the different sizes of the alanine and tyrosine side chains.

The inorganic nodes in **5-6** are $Cd_2(COO)_4N_4$ clusters seen previously in **1-3**. As before, the clusters are linked by pairs of $TMXxx^{2-}$ ligands to form 1D double chains, with bpee ligands extending from the axial positions of each cluster. However, unlike in **1-3** where the bpee ligands on every cluster are oriented parallel to each other, the double chains in **5-6** adopt a twisted conformation, causing the orientation of the bpee co-ligands of adjacent clusters to alternate along the length of the chain (**Figure 5a**). Consequently, each chain is linked to four neighbouring chains to form a 3D framework.

In **6**, the bpee ligands bonded to adjacent clusters are oriented at approximately 90° to each other, whereas in **5**, there is a distortion from orthogonality, with the corresponding angle being approximately 53°. This has a significant effect on the packing of the framework. In **6**, the orthogonal arrangement of the bpee ligands results in the formation of undulating channels with a solvent-accessible volume of 51%. In contrast, **5** contains compressed rhombic channels, with a significantly reduced void volume of 18% (**Figure 5b**). These differences may arise from the sterically bulky phenol side chain of tyrosine compared to the smaller methyl side chain of alanine, which prevents the $TMTyr^{2-}$ ligands from adopting the close packed arrangement obtained with $TMAla^{2-}$ ligands. Due to the disordered nature of the solvent molecules in the channels, the solvent mask routine[38] was used in the refinement of **5** and **6**. The structure of **5** was calculated to contain 207 residual electrons per asymmetric unit, corresponding to 2 DMF and 12.2 H_2O molecules. **6** contained 303 residual electrons, which is significantly higher than the 212 electrons calculated based on the proposed solvent content of 1.8 DMF and 7.8 methanol molecules. This could be due to the large channel size, which may facilitate loss of volatile solvent molecules in the samples prior to elemental analysis.

The TGA traces of **5** and **6** both contain a series of stepwise mass losses. In **5**, the first mass loss of 6.9% occurs gradually between 30 and 150 °C, corresponding to 9.5 H_2O molecules, followed by a second sharper mass loss of 3% from 170-245 °C, corresponding to 1 DMF molecule, before framework decomposition occurs above 265 °C. In **6**, the mass losses occur at 30-90 °C (4.0%, 2 MeOH molecules), 95-225 °C (6.2%, 3.1 MeOH molecules) and 280-335 °C (13.1%, 1.8 DMF

and 2.5 MeOH molecules). There is a short plateau in the TGA trace from 335-350 °C before framework decomposition occurs.

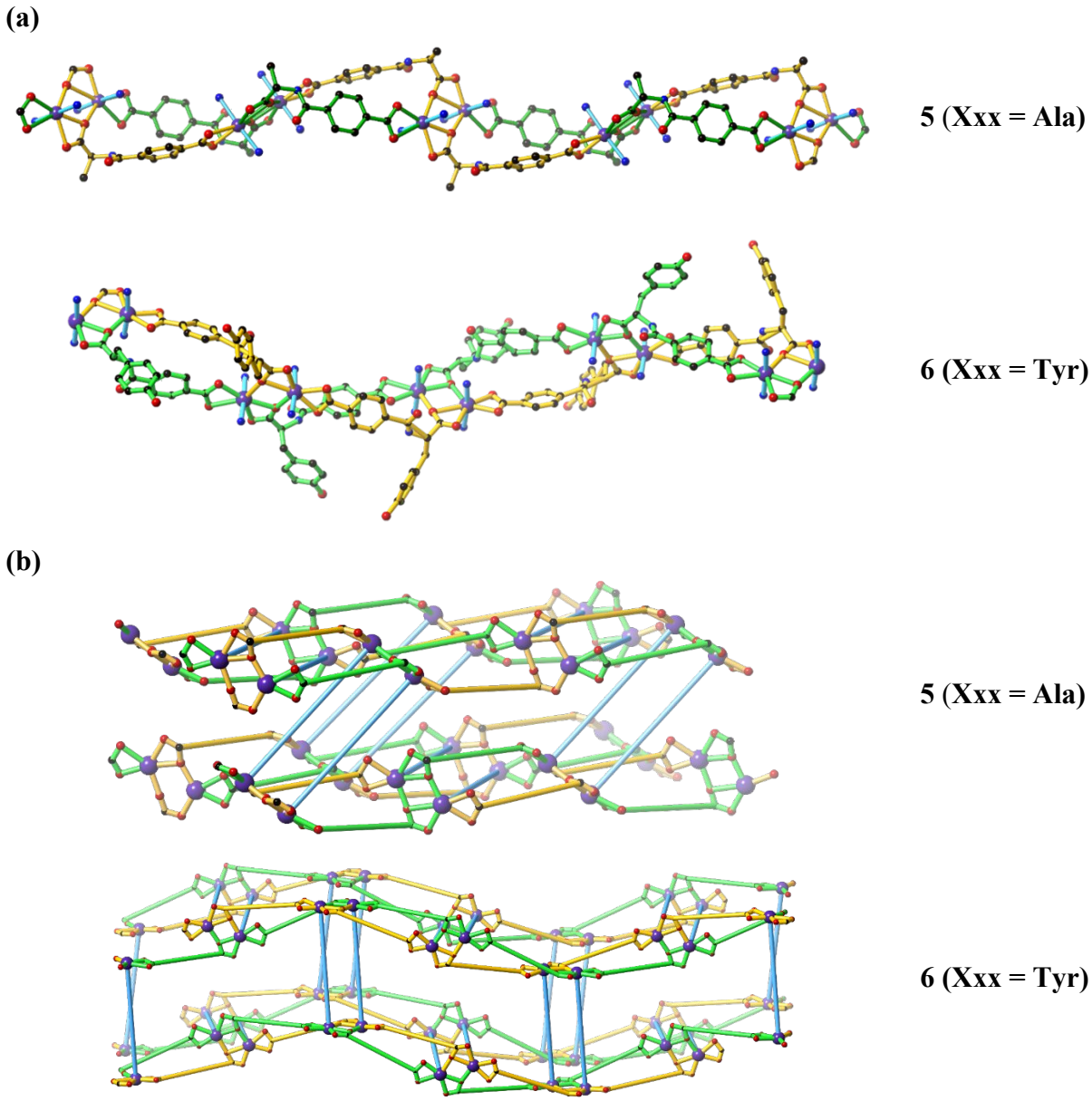

Figure 5. (a) A view of the twisted double chains in **5** (top) and **6** (bottom) with the Cd-N bonds (shown in blue) alternating in direction between adjacent clusters. The green and yellow bonds each depict one of the two chains present. For clarity, only the nitrogen centres of the bpee ligands are shown. (b) A simplified representation of the 3D frameworks in 5 (top) and 6 (bottom), with the TMXxx ligands shown as green and yellow rods and the bpee ligands as blue rods.

A 3D network obtained with H_2TMHis (7).

Despite the structural diversity of **1-6**, several recurring motifs were apparent; all six compounds contain di- or trinuclear Cd(II) clusters linked by anti-parallel pairs of $TMXxx^{2-}$ ligands into

double chains. The double chains were bridged by bpee co-ligands to obtain either 2D or 3D networks. When H_2TMHis was used as the chiral ligand, a completely different 3D framework formed. This is due to the presence of the imidazole side chain, where the N-donors readily coordinates to metal centres.

Combining H_2TMHis with bpee and $Cd(NO_3)_2 \cdot 4H_2O$ in DMF/H_2O at 80 °C resulted in the formation of colourless rectangular block crystals of composition [Cd(TMHis)(bpee)] (**7**), which crystallised in the orthorhombic space group $P2_12_12_1$ (**Figure 6**). In the structure of **7**, the $TMHis^{2-}$ ligands act as three-connecting linkers through the two carboxylate groups and one imidazole side chain (**Figure 6a**). In further contrast to compounds **1-6**, the inorganic node of **7** is a single six-coordinate Cd(II) ion with a highly distorted octahedral coordination geometry (**Figure 6b**).[39] One of the four equatorial sites is occupied by an imidazole nitrogen atom from a $TMHis^{2-}$ ligand with a Cd(II)-N distance of 2.280(7) Å. The other three equatorial sites are occupied by oxygen atoms from the carboxylate groups of two other $TMHis^{2-}$ ligands. One of the carboxylate groups binds in a chelating mode with Cd(II)-O bond distances of 2.365(5) Å and 2.571(5) Å. In the second carboxylate, one of the oxygen atoms is tightly coordinated to the Cd(II) centre with a Cd(II)-O distance of 2.280(4) Å, while the second oxygen atom is situated 2.722(5) Å from the Cd(II) centre and is likely to be involved in a long-ranged Cd(II)-O interaction. These $TMHis^{2-}$ ligands connect each cadmium atom to three other Cd(II) centres to form a corrugated 2D sheet with a (6,3)-network topology in the *ac* plane (**Figure 6c**).

The two apical sites of each Cd(II) are coordinated by bpee ligands (Cd(II)-N distances of 2.356(6) Å and 2.338(6) Å), which act as pillars that connect adjacent (6,3)-sheets to form a 3D framework with **hms** topology (**Figure 6d**).[41] Due to the large intraframework space, the framework undergoes two-fold interpenetration to generate a dense structure with no solvent-accessible voids (**Figure 6e**). The TGA trace of **7** indicates at mass loss of 7.4% from 30-100 °C, corresponding to 3 H_2O molecules. Above 100 °C, the TGA trace decreases continuously, indicating gradual decomposition of the framework. The formation of this two-fold interpenetrated 3D framework when $TMHis^{2-}$ ligands are used, elegantly demonstrates that the choice of the amino acid precursor can drastically alter the structure of the resulting framework.

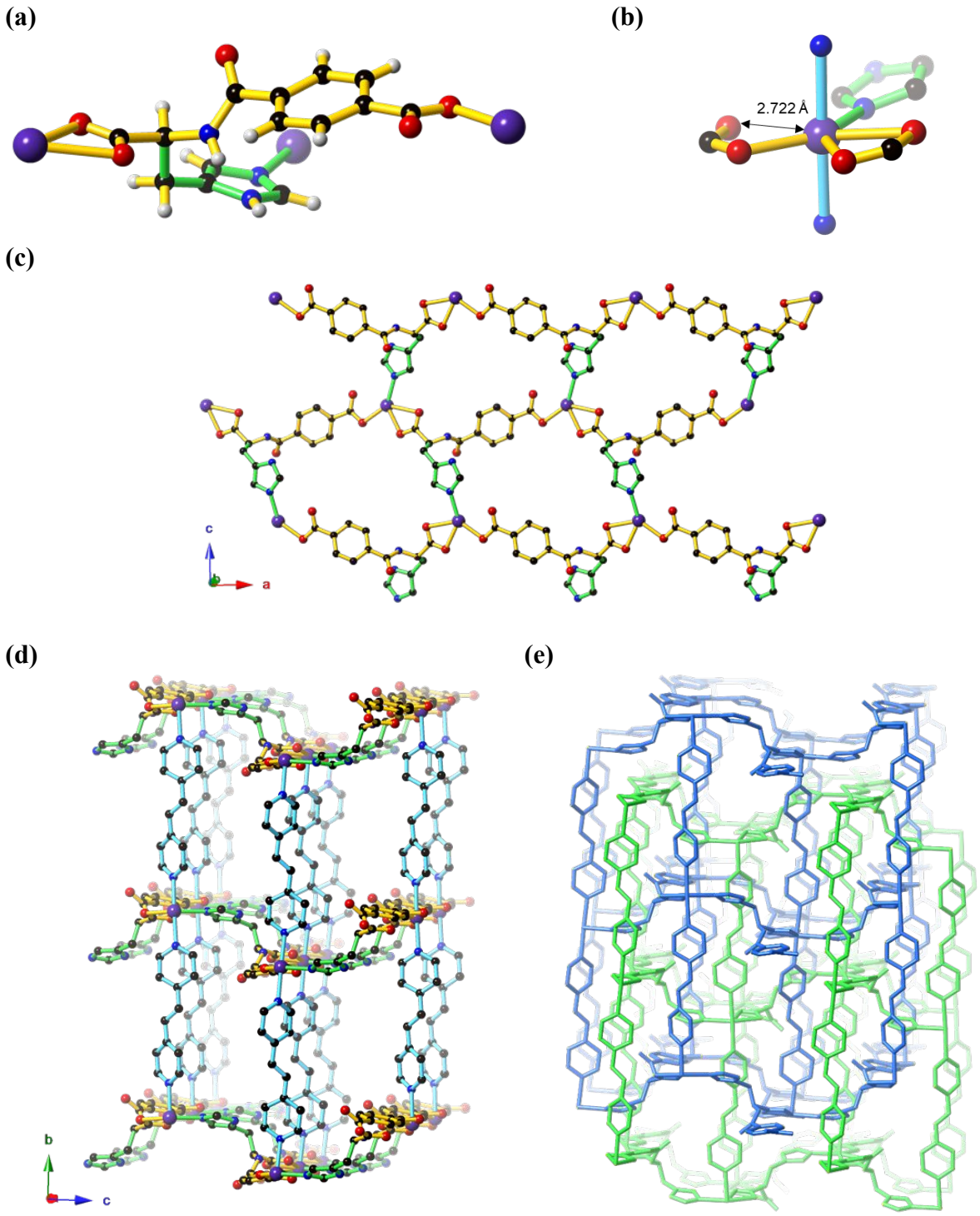

Figure 6. Structure of [Cd(TMHis)(bpee)] (**7**) showing (a) $TMHis^{2-}$ acting as a three-connecting linker, with the imidazole side chain shown in green, (b) the seven-coordinate Cd(II) centre in **7**, (c) a view of a corrugated 2D sheet containing Cd(II) centres linked by $TMHis^{2-}$ ligands (d) A single 3D framework of **7** with the bpee pillars shown in blue, (e) A stick representation of the two-fold interpenetrating frameworks in **7**, with the two independent frameworks shown in blue and green. Atoms are depicted as follows for a-d: cadmium (purple), oxygen (red), nitrogen (blue) and carbon (black). Hydrogens have been omitted for clarity.

Conclusion

In this work, a systematic study was conducted to investigate the effect of the amino acid side chain on the structure of the homochiral coordination polymers containing semi-rigid amino acid derivatives. The amino acids selected possess side chains containing aliphatic groups (alanine and valine), aromatic groups (tryptophan, tyrosine and phenylalanine) and coordinating groups (histidine). Using Cd(II) as the metal ion and bpee as a co-ligand, a series of 2D and 3D homochiral coordination polymers were obtained. When ligands derived from valine, tyrosine and tyrosine were used, three isostructural (4,4)-networks (**1**-**3**) were obtained. Despite the identical connectivity within the networks, the different intermolecular interactions formed by the side chains exerted a subtle influence on crystal packing and symmetry. The use of tryptophan led to a topologically identical framework constructed from trinuclear Cd(II) clusters and possessing a larger void space, possibly due to the greater steric bulk of the indole side chain. The use of alanine- and tyrosine-derived ligands surprisingly led to a pair of topologically identical 3D frameworks (**5**-**6**). The large different in steric bulk of the side chains significantly altered the framework geometry, resulting in channels of different shape and volume. The most dramatic structure-directing effect of the side chain was observed in the histidine-containing framework (**7**), in which the chiral ligand and metal centre both act as three-connecting nodes to form a pillared 3D structure stabilized by interpenetration.

Acknowledgements

We thank A/Prof. Brendan Abrahams for guidance, helpful discussions and feedback during this work. C.H. gratefully acknowledges the University of Melbourne for a McKenzie Fellowship. H.M.T. gratefully acknowledges the Australian Commonwealth Government and the University of Melbourne for a Research Training Programme Scholarship as well as the University of Melbourne for a Rowden White Scholarship and an Elizabeth and Vernon Puzey Scholarship. This research was undertaken on the MX1 beamline at the Australian Synchrotron, part of ANSTO.

Electronic Supplementary Information

Crystallographic and structural details, powder XRD, thermal gravimetric analysis and ATR-FTIR spectra. The crystallographic information files can be obtained from the Cambridge Structural Database: CCDC 1994309-1994315, 1994343.

Conflict of Interest Disclosure

The authors declare no competing financial interest.

References

1. Lin, G.; You, Q. D.; Cheng, J. F., Overview of Chirality and Chiral Drugs. In *Chiral Drugs*, Sons, J. W., Ed. Somerset, United States, 2011; pp 3-28.
2. Eichelbaum, M.; Gross, A. S., Stereochemical aspects of drug action and disposition. In *Advances in Drug Research*, Testa, B.; Meyer, U. A., Eds. Academic Press: 1996; Vol. 28, pp 1-64.
3. Zhang, X.; Yin, J.; Yoon, J., Recent Advances in Development of Chiral Fluorescent and Colorimetric Sensors. *Chem. Rev.* **2014,** 114, 4918-4959.
4. Sholl, D. S.; Gellman, A. J., Developing chiral surfaces for enantioselective chemical processing. *AIChE J.* **2009,** 55, 2484-2490.
5. Singh, N.; Sharma, L., Enantioseparation of D- and L- isomers of chiral drugs for improving their bioavailability: some techniques including micellization with gemini surfactants. *Indian J. Pharm. Educ. Res.* **2018,** 52, 334-341.
6. Rekoske, J. E., Chiral separations. *AIChE J.* **2001,** 47, 2-5.
7. Baiker, A., Chiral catalysis on solids. *Curr. Opin. Solid State Mater. Sci.* **1998,** 3, 86-93.
8. Falkowski, J. M.; Sawano, T.; Zhang, T.; Tsun, G.; Chen, Y.; Lockard, J. V.; Lin, W., Privileged Phosphine-Based Metal-Organic Frameworks for Broad-Scope Asymmetric Catalysis. *J. Am. Chem. Soc.* **2014,** 136, 5213-5216.
9. Ma, L.; Falkowski, J. M.; Abney, C.; Lin, W., A series of isoreticular chiral metal–organic frameworks as a tunable platform for asymmetric catalysis. *Nat. Chem.* **2010,** 2, 838.
10. Nguyen, K. D.; Kutzscher, C.; Drache, F.; Senkovska, I.; Kaskel, S., Chiral Functionalization of a Zirconium Metal-Organic Framework (DUT-67) as a Heterogeneous Catalyst in Asymmetric Michael Addition Reaction. *Inorg. Chem.* **2018,** 57, 1483-1489.
11. Xi, W.; Liu, Y.; Xia, Q.; Li, Z.; Cui, Y., Direct and Post-Synthesis Incorporation of Chiral Metallosalen Catalysts into Metal-Organic Frameworks for Asymmetric Organic Transformations. *Chem. Eur. J.* **2015,** 21, 12581-12585.
12. Dong, X. W.; Yang, Y.; Che, J. X.; Zuo, J.; Li, X. H.; Gao, L.; Hu, Y. Z.; Liu, X. Y., Heterogenization of homogeneous chiral polymers in metal-organic frameworks with enhanced catalytic performance for asymmetric catalysis. *Green Chem.* **2018,** 20, 4085-4093.
13. Xiong, R. G.; You, X. Z.; Abrahams, B. F.; Xue, Z.; Che, C. M., Enantioseparation of Racemic Organic Molecules by a Zeolite Analogue. *Angew. Chem. Int. Ed.* **2001,** 40, 4422-4425.
14. Tanaka, K.; Muraoka, T.; Otubo, Y.; Takahashi, H.; Ohnishi, A., HPLC enantioseparation on a homochiral MOF–silica composite as a novel chiral stationary phase. *RSC Adv.* **2016,** 6, 21293-21301.
15. Zhuo, C.; Wen, Y.; Hu, S.; Sheng, T.; Fu, R.; Xue, Z.; Zhang, H.; Li, H.; Yuan, J.; Chen, X.; Wu, X., Homochiral Metal–Organic Frameworks with Tunable Nanoscale

Channel Array and Their Enantioseparation Performance against Chiral Diols. *Inorg. Chem.* **2017,** 56, 6275-6280.

16. Padmanaban, M.; Müller, P.; Lieder, C.; Gedrich, K.; Grünker, R.; Bon, V.; Senkovska, I.; Baumgärtner, S.; Opelt, S.; Paasch, S.; Brunner, E.; Glorius, F.; Klemm, E.; Kaskel, S., Application of a chiral metal–organic framework in enantioselective separation. *Chem. Commun.* **2011,** 47, 12089-12091.
17. Zhou, H. C.; Long, J. R.; Yaghi, O. M., Introduction to Metal–Organic Frameworks. *Chem. Rev.* **2012,** 112, 673-674.
18. Han, Z.; Shi, W.; Cheng, P., Synthetic strategies for chiral metal-organic frameworks. *Chin. Chem. Lett.* **2018,** 29, 819-822.
19. Liu, Y.; Xuan, W.; Cui, Y., Engineering Homochiral Metal-Organic Frameworks for Heterogeneous Asymmetric Catalysis and Enantioselective Separation. *Adv. Mater.* **2010,** 22, 4112-4135.
20. Wu, C. D.; Hu, A.; Zhang, L.; Lin, W., A Homochiral Porous Metal−Organic Framework for Highly Enantioselective Heterogeneous Asymmetric Catalysis. *J. Am. Chem. Soc.* **2005,** 127, 8940-8941.
21. Grosshans, P.; Jouaiti, A.; Bulach, V.; Planeix, J. M.; Hosseini, M. W.; Nicoud, J. F., Molecular tectonics: from enantiomerically pure sugars to enantiomerically pure triple stranded helical coordination network. *Chem. Commun.* **2003,** 1336-1337.
22. Barron, J. A.; Glazier, S.; Bernhard, S.; Takada, K.; Houston, P. L.; Abruña, H. D., Photophysics and redox behavior of chiral transition metal polymers. *Inorg. Chem.* **2003,** 42, 1448-1455.
23. Gruselle, M.; Thouvenot, R.; Malézieux, B.; Train, C.; Gredin, P.; Demeschik, T. V.; Troitskaya, L. L.; Sokolov, V. I., Enantioselective Self-Assembly of Bimetallic $[Mn^{II}(\Delta)$-$Cr^{III}(C_2O_4)_3]-$ and $[Mn^{II}(\Lambda)$-$Cr^{III}(C_2O_4)_3]-$ Layered Anionic Networks Templated by the Optically Active (Rp)- and (Sp)-$[1\text{-}CH_2N(n\text{-}C_3H_7)_3\text{-}2\text{-}CH_3C_5H_3FeC_5H_5]^+$ Ions. *Chem. Eur. J.* **2004,** 10, 4763-4769.
24. Train, C.; Gheorghe, R.; Krstic, V.; Chamoreau, L. M.; Ovanesyan, N. S.; Rikken, G. L. J. A.; Gruselle, M.; Verdaguer, M., Strong magneto-chiral dichroism in enantiopure chiral ferromagnets. *Nat. Mater.* **2008,** 7, 729-734.
25. Lin, Z.; Slawin, A. M. Z.; Morris, R. E., Chiral Induction in the Ionothermal Synthesis of a 3-D Coordination Polymer. *J. Am. Chem. Soc.* **2007,** 129, 4880-4881.
26. Hailili, R.; Wang, L.; Qv, J.; Yao, R.; Zhang, X. M.; Liu, H., Planar Mn_4O Cluster Homochiral Metal–Organic Framework for HPLC Separation of Pharmaceutically Important (±)-Ibuprofen Racemate. *Inorg. Chem.* **2015,** 54, 3713-3715.
27. Liang, X. Q.; Li, D. P.; Zhou, X. H.; Sui, Y.; Li, Y. Z.; Zuo, J. L.; You, X. Z., Metal−Organic Coordination Polymers Generated from Chiral Camphoric Acid and Flexible Ligands with Different Spacer Lengths: Syntheses, Structures, and Properties. *Cryst. Growth Des.* **2009,** 9, 4872-4883.
28. Gu, Z. G.; Zhan, C.; Zhang, J.; Bu, X., Chiral chemistry of metal–camphorate frameworks. *Chem. Soc. Rev.* **2016,** 45, 3122-3144.
29. Pu, F.; Liu, X.; Xu, B.; Ren, J.; Qu, X., Miniaturization of Metal–Biomolecule Frameworks Based on Stereoselective Self-Assembly and Potential Application in Water Treatment and as Antibacterial Agents. *Chem. Eur. J.* **2012,** 18, 4322-4328.

30. Guan, G. X.; Liu, X.; Yue, Q.; Gao, E. Q., Homochiral Metal–Organic Frameworks Embedding Helicity Based on a Semirigid Alanine Derivative. *Cryst. Growth Des.* **2018,** 18, 364-372.
31. Xu, Z. X.; Tan, Y. X.; Fu, H. R.; Liu, J.; Zhang, J., Homochiral Metal–Organic Frameworks with Enantiopure Proline Units for the Catalytic Synthesis of β-Lactams. *Inorg. Chem.* **2014,** 53, 12199-12204.
32. Rebilly, J. N.; Bacsa, J.; Rosseinsky, M. J., 1 D Tubular and 2 D Metal–Organic Frameworks Based on a Flexible Amino Acid Derived Organic Spacer. *Chem. Asian J.* **2009,** 4, 892-903.
33. McPhillips, T. M.; McPhillips, S. E.; Chiu, H. J.; Cohen, A. E.; Deacon, A. M.; Ellis, P. J.; Garman, E.; Gonzalez, A.; Sauter, N. K.; Phizackerley, R. P.; Soltis, S. M.; Kuhn, P., Blu-Ice and the Distributed Control System: software for data acquisition and instrument control at macromolecular crystallography beamlines. *J. Synchrotron Radiat.* **2002,** 9, 401-406.
34. Aragao, D.; Aishima, J.; Cherukuvada, H.; Clarken, R.; Clift, M.; Cowieson, N. P.; Ericsson, D. J.; Gee, C. L.; Macedo, S.; Mudie, N.; Panjikar, S.; Price, J. R.; Riboldi-Tunnicliffe, A.; Rostan, R.; Williamson, R.; Caradoc-Davies, T. T., MX2: a high-flux undulator microfocus beamline serving both the chemical and macromolecular crystallography communities at the Australian Synchrotron. *J. Synchrotron Radiat.* **2018,** 25, 885-891.
35. Sheldrick, G., SHELXT - Integrated space-group and crystal-structure determination. *Acta Cryst. A* **2015,** 71, 3-8.
36. Sheldrick, G., Crystal structure refinement with SHELXL. *Acta Cryst. C* **2015,** 71, 3-8.
37. Dolomanov, O. V.; Bourhis, L. J.; Gildea, R. J.; Howard, J. A. K.; Puschmann, H., OLEX2: a complete structure solution, refinement and analysis program. *J. Appl. Crystallogr.* **2009,** 42, 339-341.
38. Van Der Sluis, P.; Spek, A. L., BYPASS: an effective method for the refinement of crystal structures containing disordered solvent regions. *Acta Cryst. A* **1990,** *46* (3), 194-201.
39. Llunell, M.; Casanova, D.; Cicera, J.; Alemany, P.; Alvarez, S. *SHAPE*, 2.1; Barcelona, Spain, 2013.
40. Groom, C. R.; Bruno, I. J.; Lightfoot, M. P.; Ward, S. C., The Cambridge Structural Database. *Acta Cryst. B* **2016,** 72, 171-179.
41. Blatov, V. A.; Shevchenko, A. P.; Proserpio, D. M., Applied Topological Analysis of Crystal Structures with the Program Package ToposPro. *Cryst. Growth Des.* **2014,** 14, 3576-3586.
42. Burrows, A. D.; Cassar, K.; Friend, R. M. W.; Mahon, M. F.; Rigby, S. P.; Warren, J. E., Solvent hydrolysis and templating effects in the synthesis of metal–organic frameworks. *CrystEngComm* **2005,** 7, 548-550.

For Table of Contents Use Only:

Chiral Cd(II) coordination polymers based on amino acid derivatives: the effect of side chain on structure

*Hui Min Tay and Carol Hua**

School of Chemistry, The University of Melbourne, Parkville, Victoria, 3010, Australia. *E-mail: carol.hua@unimelb.edu.au

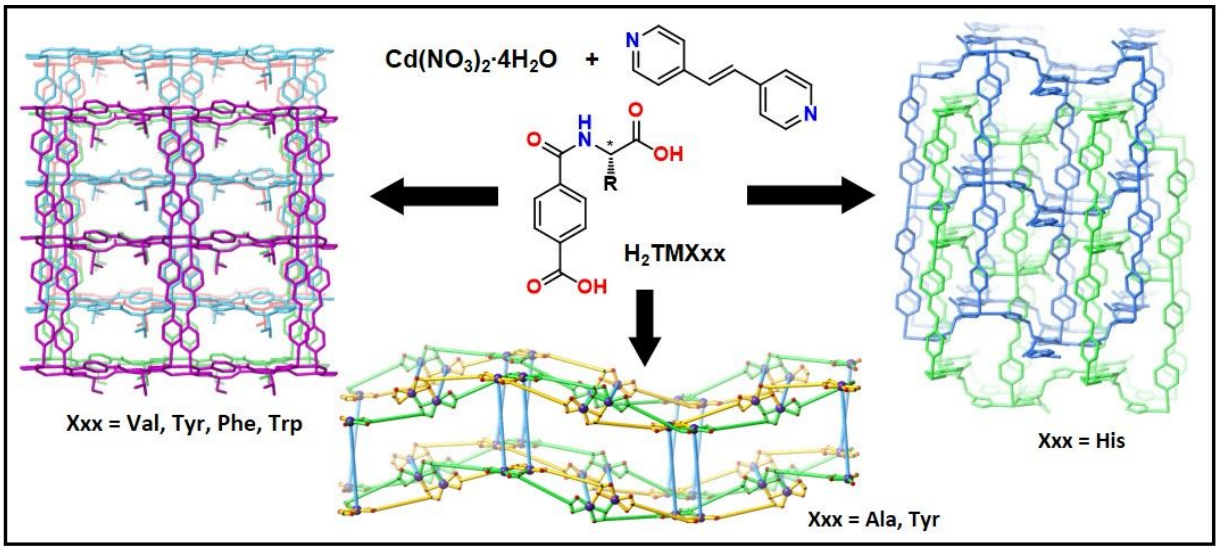

Seven homochiral Cd(II) coordination polymers were generated using dicarboxylates composed of L-amino acids appended to terephthalic acid. 2D networks were obtained using ligands derived from valine, tyrosine, phenylalanine and tryptophan while 3D frameworks were generated from alanine, tyrosine and histidine. The side chain influenced both network connectivity and crystal packing.